ChemComm

COMMUNICATION

View Article Online
View Journal | View Issue

Cite this: *Chem. Commun.*, 2017, 53, 3373

Received 8th February 2017,
Accepted 27th February 2017

DOI: 10.1039/c7cc01019b

rsc.li/chemcomm

Graphene oxide-enhanced cytoskeleton imaging and mitosis tracking†

Qian-Ru Li,‡[a] Jin-Biao Jiao,‡[b] Li-Li Li,[c] Xiao-Peng He,*[b] Yi Zang,*[c] Tony D. James,[d] Guo-Rong Chen,[b] Lin Guo*[a] and Jia Li*[c]

Here we show that graphene oxide greatly enhances the imaging ability of a peptide probe that selectively targets microtubules of the cytoskeleton, thus enabling the dynamic tracking of mitosis in live cells.

Microtubules, a key component of the cytoskeleton, are composed of polymerized α- and β-tubulin dimers. Their dynamic polymerization is involved in a variety of cellular processes including mitosis, cytokinesis, polarity and vesicular transport.[1,2] Microtubule tracks are covered with microtubule-associated proteins (MAPs), which contribute to their stability and thus play important roles in maintaining normal functions of the microtubules. The best-studied members of the MAPs are MAP4, tau and MAP2.[3,4]

To date, the most widely used microtubule probe is fluorophore-linked taxane.[5] However, while the use of drugs as a targeting agent for cell imaging may cause toxicity concerns leading to dysfunction of the cells (resulting in an inability to track the normal physiological processes of live cells), probes based on the more biocompatible and versatile peptides with specific microtubule-binding motifs have been rarely used. In 1988, an 18-amino-acid peptide that targets a microtubule binding site shared by MAP2 and tau was reported.[6] By using the major-coat phage display technique, a specific microtubule-binding peptide for MAPs has been identified.[7] However, the tubulin-binding affinity of these peptide ligands has only been confirmed *in vitro* (*i.e.* using transmission electron microscopy to determine the interaction between affinity-selected tubulin-binding phage and tubulins).[7] This is largely due to the poor membrane permeability of some peptides and the lack of reliable imaging materials for spatiotemporal tracking of microtubules in live cells.

Graphene oxide (GO), a two-dimensional material, has recently been extensively used for biomedical applications.[8–16] The large surface area of GO and its unique optical properties makes the construction of ligand-attached GO material composites for targeted imaging of cells and intracellular macromolecules possible.[16] In particular, we have demonstrated that GO can greatly enhance the imaging ability of fluorophore-tagged ligands for cells that express a selective transmembrane receptor.[17,18] Here we show that GO has the ability to enhance the cytoskeleton imaging ability of a membrane–impermeable peptide ligand selective for microtubules, thus enabling the dynamic tracking of mitosis in live cells (Fig. 1).

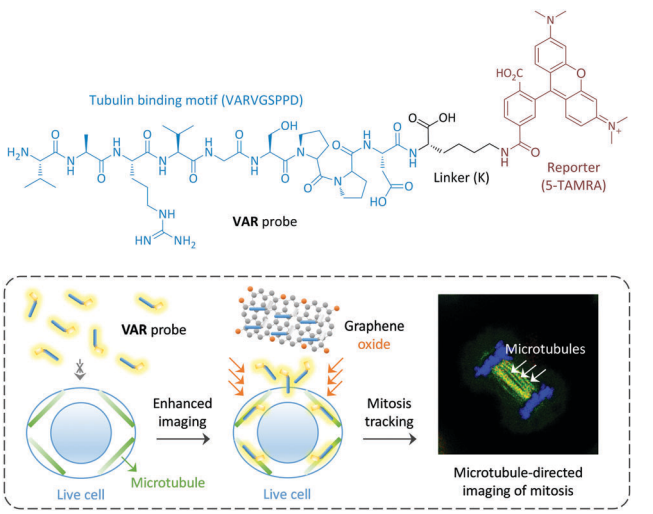

Fig. 1 Structure of the peptide-ligand-based **VAR** probe and schematic illustration of graphene oxide enhanced, microtubule-targeted imaging of live cells and tracking of cell mitosis.

[a] *State Key Laboratory of Virology, College of Life Sciences, Wuhan University, Wuhan, 430072, P. R. China. E-mail: guol@whu.edu.cn*
[b] *Key Laboratory for Advanced Materials & Institute of Fine Chemicals, School of Chemistry and Molecular Engineering, East China University of Science and Technology, Shanghai 200237, P. R. China. E-mail: xphe@ecust.edu.cn*
[c] *National Center for Drug Screening, State Key Laboratory of Drug Research, Shanghai Institute of Materia Medica, Chinese Academy of Sciences, 189 Guo Shoujing Rd., Shanghai 201203, P. R. China. E-mail: yzang@simm.ac.cn, jli@simm.ac.cn*
[d] *Department of Chemistry, University of Bath, Bath, BA2 7AY, UK*

† Electronic supplementary information (ESI) available: Additional figures and experimental section. See DOI: 10.1039/c7cc01019b

‡ Equal contribution.

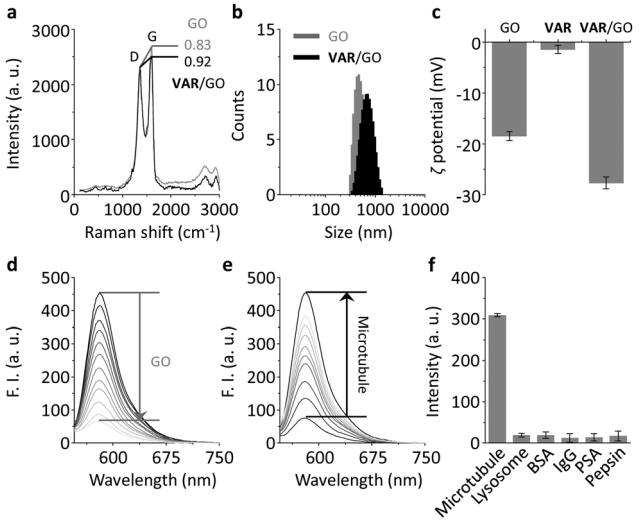

Fig. 2 (a) Raman spectroscopy of GO (30 μg mL^{-1}) and **VAR**/GO (1.5 μM/30 μg mL^{-1}). (b) Dynamic light scattering of GO (9.1 μg mL^{-1}) and **VAR**/GO (0.5 μM/9.1 μg mL^{-1}). (c) Zeta (ζ) potential of **VAR** probe (0.5 μM), GO (9.1 μg mL^{-1}) and **VAR**/GO (0.5 μM/9.1 μg mL^{-1}). (d) Fluorescence spectra of **VAR** probe (0.5 μM) in the presence of increasing GO (0–9.1 μg mL^{-1}). (e) Fluorescence spectra of **VAR**/GO (0.5 μM/9.1 μg mL^{-1}) in the presence of increasing microtubule (0–29.56 nM). (f) Fluorescence intensity of **VAR**/GO (0.5 μM/9.1 μg mL^{-1}) in the presence of microtubule (29.56 nM) and other proteins (30 nM) (BSA = bovine serum albumin; PSA = pisum sativum agglutinin; IgG = immunoglobulin G). All fluorescence measurements were carried out in phosphate buffered saline (0.01 M, pH 7.4) at room temperature with an excitation wavelength of 510 nm.

We used a microtubule-selective peptide ligand (VARVGSPPD) obtained by the phage display technique,[7] to which a fluorescent reporter (5-carboxytetramethylrhodamine (5-TAMRA)) was introduced through L-arginine (K) (Fig. 1). With the probe in hand, we first tested its interaction with GO (produced by the modified Hummer's method)[19,20] in phosphate buffered saline. The morphology of the GO was characterized using transmission electron microscopy (Fig. S1, ESI†). As determined by Raman spectroscopy, the I_D/I_G (intensity of D band to that of G band) ratio of GO increased with **VAR** probe (Fig. 2a), suggesting that the attachment of the peptide to GO perturbed the C-sp^2-hybridization order of the material surface.[11] The size of **VAR**/GO increased with respect to GO alone as shown by dynamic light scattering (Fig. 2b), and addition of **VAR** probe to GO significantly changed the zeta potential of the latter (Fig. 2c).

We also used fluorescence spectroscopy to characterize the binding between the probe and material. The fluorescence of the **VAR** probe gradually decreased with increasing GO (Fig. 2d), which was probably a result of Förster resonance energy transfer between the two closely conjugated species.[21] However, the presence of microtubule (taxol-stabilized microtubule that is polymerized by α/β tubulins) gradually recovered the peptide fluorescence (Fig. 2e) with good linearity (Fig. S2a, ESI†). The limit of detection of **VAR**/GO for microtubule was determined to be as low as 2.4 pM. This ultra-sensitivity suggests a strong binding affinity between the peptide ligand and microtubules, setting a basis for the facile *in vitro* screening of other microtubule binders using the **VAR**/GO material system. A kinetic assay indicated that the fluorescence recovery of the **VAR** probe with microtubule quickly reached equilibrium within 15 min (Fig. S2b, ESI†). The fact that the presence of a range of unselective proteins did not enhance the fluorescence of the material composite suggests a good biospecificity of the peptide ligand (Fig. 2f and Fig. S2c, ESI†). To further corroborate the selective ligand–microtubule binding, a competition assay was performed. In the presence of GO and microtubule, the addition of increasing free peptide ligand (VARVGSPPD) gradually decreased the fluorescence of the **VAR** probe (Fig. S3, ESI†), suggesting the specific association between the probe and protein.

Having determined the specific binding between the **VAR** probe and microtubule as facilitated by GO, we then set out to test the imaging ability of the probe for the cell cytoskeleton. HeLa cells expressing EGFP-α tubulin (EGFP = enhanced green fluorescence protein), established in a previous report, were utilised.[22] Using EGFP fluorescence as a reference, we first observed that treatment of just the **VAR** probe with the cells did not lead to any obvious concentration-dependent production of probe (TAMRA) fluorescence intracellularly (Fig. S4, ESI†), suggesting poor cell permeability of the peptide probe. In contrast, the presence of GO significantly enhanced the imaging ability of the **VAR** probe in both a dose (Fig. 3a and c) and time-dependent manner (Fig. 3b and d). Both the GO material and **VAR** probe were determined to be not toxic to HeLa with increasing concentrations (Fig. S5, ESI†).

Furthermore, we used an alternative cell line (human embryonic kidney 293T) transfected with EGFP-α-tubulin to investigate the generality of the developed method. TAMRA fluorescence was only observed for the **VAR**/GO ensemble and not the free **VAR** probe and GO (Fig. S6, ESI†). These observations are comparable to those observed for HeLa cells, indicating the broad applicability of GO for enhancing microtubule-targeted imaging of peptide probes. These results are in agreement with the excellent intracellular delivery ability of GO for small-molecular drugs, peptides and aptamers.[16,18,23,24,31–34]

To test whether the **VAR** probe could bind dynamic mitotic microtubules intracellularly, a confocal laser scanning microscope was used. We first determined that the EGFP-α-tubulin fluorescence localized well with that of TAMRA, suggesting that the probe was probably bound to the polymerized tubulins (Fig. 4). In addition, we also determined that the probe could be used for tracking the mitosis of HeLa (Fig. 4). During interphase, cells were adhered to the coverslip with a flat shape, whereas upon entering mitotic phase, mitotic apparatuses were dynamically organized by microtubules and microtubule associated proteins, including the spindle during metaphase and the central spindle during anaphase. These mitotic apparatuses were clearly visualized by the **VAR** probe.

In summary, we have shown that GO enhances the cytoskeleton imaging ability of a cell-impermeable peptide ligand for microtubules, thus enabling the dynamic tracking of mitosis in live cells. This research provides insights into the use of 2D materials for enabling imaging and spatiotemporal tracking of cell fate by peptide probes. Our ongoing research will focus on

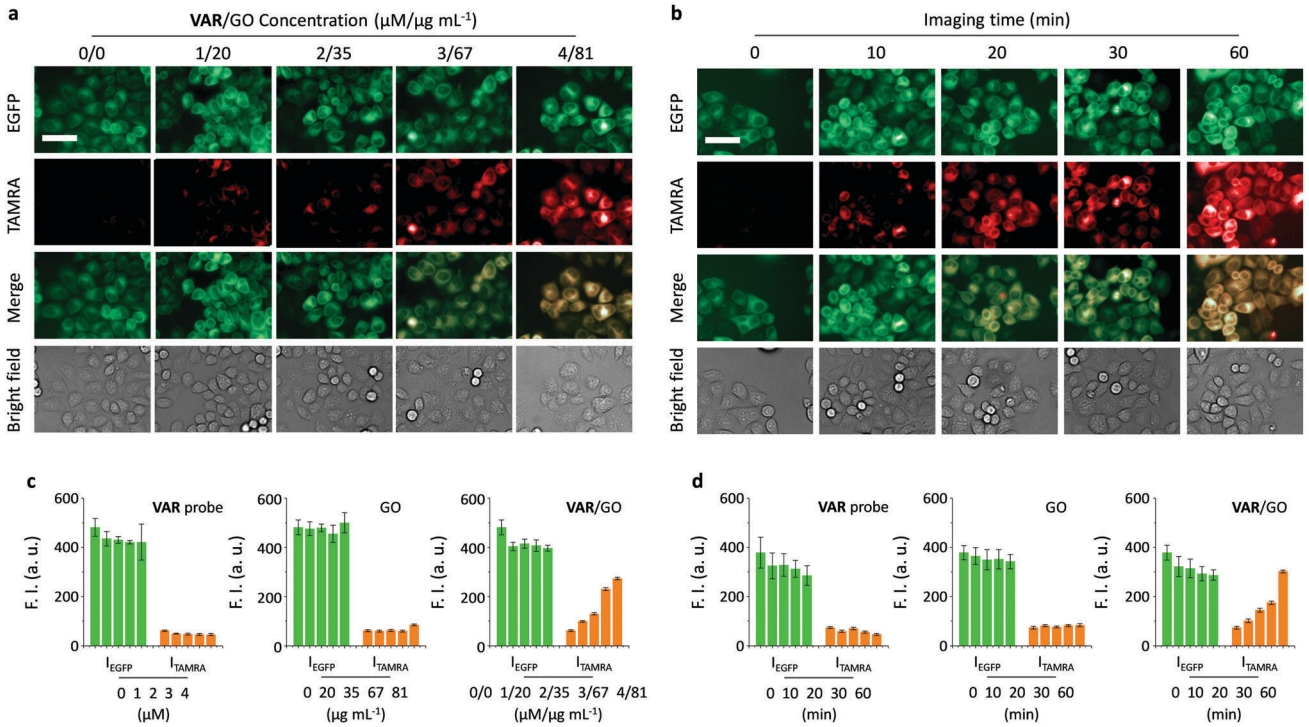

Fig. 3 Dose-dependent fluorescence imaging (a) and quantification (c) of **VAR** probe, GO and **VAR**/GO for HeLa cells stably expressing EGFP-α tubulin. Time-dependent fluorescence imaging (b) and quantification (d) of **VAR** probe (4 μM), GO (81 μg mL^{-1}) and **VAR**/GO (4 μM/81 μg mL^{-1}) for HeLa cells stably expressing EGFP-α tubulin. Excitation channels for EGFP and TAMRA are 460–490 and 520–550 nm, and emission channels for EGFP and TAMRA are 500–540 and 560–630 nm, respectively. Scale bar = 50 μm (applicable to all images).

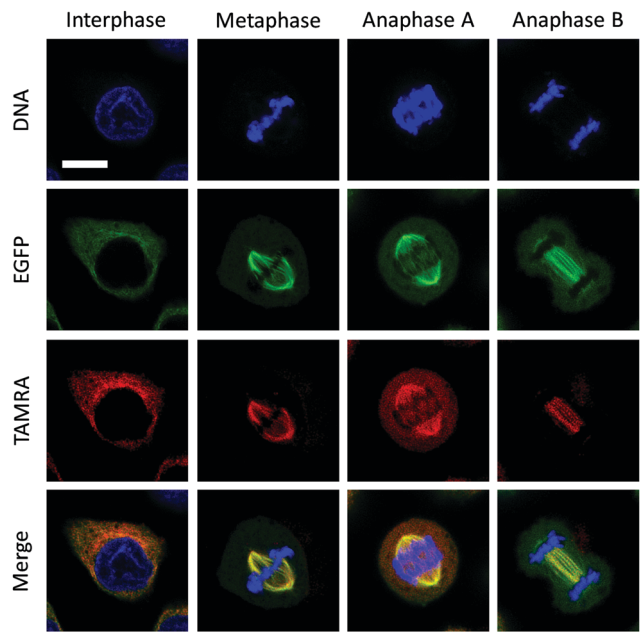

Fig. 4 Imaging of mitosis in live HeLa cells by confocal microscopy (excitation channels for DNA (stained by Hoechst), EGFP and TAMRA are 405, 488 and 525 nm, and emission channels for DNA, EGFP and TAMRA are 430–480, 490–540 and 580–620 nm, respectively). Scale bar = 10 μm (applicable to all images).

the use of other 2D materials[25–30] for peptide-based cytoskeleton imaging.

This research is supported by the 973 project (2013CB733700), the National Natural Science Foundation of China (21572058 and 21576088), the Science and Technology Commission of Shanghai Municipality (15540723800), the Shanghai Rising-Star Program (16QA1401400) (to X.-P. He) and the Shanghai Science and Technology Development Funds (14YF1413300). The Catalysis And Sensing for our Environment (CASE) net-work is thanked for research exchange opportunities. T. D. J. thanks ECUST for a guest professorship.

Notes and references

1 H. de Forges, A. Bouissou and F. Perez, *Int. J. Biochem. Cell Biol.*, 2011, **44**, 266.
2 M. Stiess and F. Bradke, *Dev. Neurobiol.*, 2011, **71**, 430.
3 L. Dehmelt and S. Halpain, *Genome Biol.*, 2005, **6**, 204.
4 S. Halpain and L. Dehmelt, *Genome Biol.*, 2006, **7**, 224.
5 G. Lukinavičius, L. Reymond, E. D'Este, A. Masharina, F. Göttfert, H. Ta, A. Güther, M. Fournier, S. Rizzo, H. Waldmann, C. Blaukopf, C. Sommer, D. W. Gerlich, H. D. Arndt, S. W. Hell and K. Johnsson, *Nat. Methods*, 2014, **11**, 731.
6 S. A. Lewis, D. H. Wang and N. J. Cowan, *Science*, 1988, **242**, 936.
7 B. Cao and C. Mao, *Biomacromolecules*, 2009, **10**, 555.
8 K. Kostarelos and K. S. Novoselov, *Science*, 2014, **344**, 261.
9 K. Yang, S. Zhang, G. Zhang, X. Sun, S.-T. Lee and Z. Liu, *Nano Lett.*, 2010, **10**, 3318.
10 L. Feng, L. Wu and X. Qu, *Adv. Mater.*, 2013, **25**, 168.
11 H.-L. Zhang, X.-L. Wei, Y. Zang, J.-Y. Cao, S. Liu, X.-P. He, Q. Chen, Y.-T. Long, J. Li, G.-R. Chen and K. Chen, *Adv. Mater.*, 2013, **25**, 4097.
12 (*a*) D.-K. Ji, G.-R. Chen, X.-P. He and H. Tian, *Adv. Funct. Mater.*, 2015, **25**, 3483; (*b*) D. Xie, X.-Q. Feng, X.-L. Hu, L. Liu, Z. Ye, J. Cao, G.-R. Chen, X.-P. He and Y.-T. Long, *ACS Appl. Mater. Interfaces*, 2016, **8**, 25137; (*c*) L. Cui, B.-W. Zhu, S. Qu, X.-P. He and G.-R. Chen, *Dyes Pigm.*, 2015, **121**, 312; (*d*) X.-P. He, Q. Deng, L. Cai, C.-Z. Wang,

Y. Zang, J. Li, G.-R. Chen and H. Tian, *ACS Appl. Mater. Interfaces*, 2014, **6**, 5379; (*e*) X. Sun, B. Zhu, D.-K. Ji, Q. Chen, X.-P. He, G.-R. Chen and T. D. James, *ACS Appl. Mater. Interfaces*, 2014, **6**, 10078.
13 K. Yang, L. Feng, H. Hong, W. Cai and Z. Liu, *Nat. Protoc.*, 2013, **8**, 2392.
14 C. Chung, Y.-K. Kim, D. Shin, S.-R. Ryoo, B. H. Hong and D.-H. Min, *Acc. Chem. Res.*, 2013, **46**, 2211.
15 V. Georgakilas, J. N. Tiwari, K. C. Kemp, J. A. Perman, A. B. Bourlinos, K. S. Kim and R. Zboril, *Chem. Rev.*, 2016, **116**, 5464.
16 For a tutorial review, see: X.-P. He, Y. Zang, T. D. James, J. Li and G.-R. Chen, *Chem. Soc. Rev.*, 2015, **44**, 4239.
17 D.-K. Ji, Y. Zhang, X.-P. He and G.-R. Chen, *J. Mater. Chem. B*, 2015, **3**, 6656.
18 D.-K. Ji, Y. Zhang, Y. Zang, W. Liu, X. Zhang, J. Li, G.-R. Chen, T. D. James and X.-P. He, *J. Mater. Chem. B*, 2015, **3**, 9182.
19 N. I. Kovtyukhova, P. J. Olivier, B. R. Martin, T. E. Mallouk, S. A. Chizhik and E. V. Buzaneva, *Chem. Mater.*, 1999, **11**, 771.
20 D. R. Dreyer, S. Park, C. W. Bielawski and R. S. Rouff, *Chem. Soc. Rev.*, 2010, **39**, 228.
21 E. Morales-Naráez and A. Merkoçi, *Adv. Mater.*, 2012, **24**, 3298.
22 T. Chinen, P. Liu, S. Shioda, J. Pagel, B. Cerikan, T.-C. Lin, O. Gruss, Y. Hayashi, H. Takeno, T. Shima, Y. Okada, I. Hayakawa, Y. Hayashi, H. Kigoshi, T. Usui and E. Schiebel, *Nat. Commun.*, 2015, **6**, 8722.
23 Y. Wang, Z. Li, D. Hu, C.-T. Lin, J. Li and Y. Lin, *J. Am. Chem. Soc.*, 2010, **132**, 9274.
24 K. Yang, L. Feng, X. Shi and Z. Liu, *Chem. Soc. Rev.*, 2013, **42**, 530.
25 D.-K. Ji, Y. Zhang, Y. Zang, J. Li, G.-R. Chen, X.-P. He and H. Tian, *Adv. Mater.*, 2016, **28**, 9356.
26 X.-P. He and H. Tian, *Small*, 2016, **12**, 144.
27 M. Wahiba, X.-Q. Feng, Y. Zang, T. D. James, J. Li, G.-R. Chen and X.-P. He, *Chem. Commun.*, 2016, **52**, 11689.
28 D. Xie, D.-K. Ji, Y. Zhang, J. Cao, H. Zheng, L. Liu, Y. Zang, J. Li, G.-R. Chen, T. D. James and X.-P. He, *Chem. Commun.*, 2016, **52**, 9418.
29 Y.-H. Ma, W.-T. Dou, Y.-F. Pan, L.-W. Dong, Y.-X. Tan, X.-P. He, H. Tian and H.-Y. Wang, *Adv. Mater.*, 2017, **29**, 1604253.
30 S. Guo, J. Chen, B.-Y. Cai, W.-W. Chen, Y.-F. Li, X. Sun, G.-R. Chen, X.-P. He and T. D. James, *Mater. Chem. Front.*, 2017, **1**, 61.
31 L. Li, J. Feng, H. Liu, Q. Li, L. Tong and B. Tang, *Chem. Sci.*, 2016, **7**, 1940.
32 H. Ji, Y. Guan, L. Wu, J. Ren, D. Miyoshi, N. Sugimoto and X. Qu, *Chem. Commun.*, 2015, **51**, 1479.
33 Z. Xu, S. Zhu, M. Wang, Y. Li, P. Shi and X. Huang, *ACS Appl. Mater. Interfaces*, 2015, **7**, 1355.
34 M. Hong, L. Xu, Q. Xue, L. Li and B. Tang, *Anal. Chem.*, 2016, **88**, 12177.

